CPML and Quasi-CPML for Cylindrical MRTD Method

Pin Zhang, Yawen Liu[*], Shi Qiu, and Bo Yang

Abstract—Two absorbing boundary conditions (ABC's) are derived for the cylindrical MRTD grids. The first one is the convolutional perfectly matched layer (CPML) based on stretched coordinates with complex frequency shifted constitutive parameters, and the other is the straightforward extension of CPML named quasi-CPML (QCPML) as it is no longer perfectly matched for cylindrical interfaces. Unlike the Berenger's PML, the implementations of the two ABC's are completely independent of the host material. Numerical results show that both ABC's can provide a quite satisfactory absorbing boundary condition, and can save more CPU time and memory than the Berenger's PML, while the QCPML has an advantage of CPML at the proposed absorbing performance, CPU time and memory saving. Moreover, it is shown that the QCPML is more effective than the PML and CPML at absorbing evanescent waves.

1. INTRODUCTION

The Multi-Resolution Time-Domain (MRTD) technique was first proposed by Krumpholz and Katehi [1, 2], and has been developed rapidly as one of the efficient numerical algorithms in the time-domain such as the long established Finite Difference Time-Domain (FDTD) technique [3–15]. In [16], the MRTD and PML-MRTD concepts have been applied to cylindrical coordinates.

In this work, the CPML [17, 18] and QCPML are derived for the cylindrical MRTD scheme. Unlike the PML in [16], the implementation of the proposed two ABC's is independent of the material medium, which implies that no matter in homogeneous, inhomogeneous, lossy, dispersive, anisotropic or nonlinear media, the implementation can be used without any further generalization. The absorbing effectiveness of both ABC's are investigated and compared with that of the PML [16, 19]. Numerical simulations show that the CPML and QCPML have a very good absorbing performance. Moreover, the requirement for CPU time and memory is also compared between PML, CPML and QCPML. It is shown that compared with the PML, both CPML and QCPML, especially the QCPML, can save more computation time and computer memory in general. It should be noticed that the compact support wavelet-Daubechies with two vanishing moments (D_2) [4, 7] is employed to the cylindrical MRTD in this work.

2. FORMULATION

2.1. MRTD for Cylindrical Grid

For simplicity, a homogeneous medium is considered. Maxwell's first vector equation is stated by

$$\nabla \times \mathbf{H} = \varepsilon \frac{\partial \mathbf{E}}{\partial t} \tag{1}$$

The MRTD solution of Maxwell's equations requires the discretization of Eq. (1). In cylindrical coordinates, Eq. (1) can be rewritten as

$$\varepsilon \frac{\partial E_\rho}{\partial t} = \frac{1}{\rho}\frac{\partial H_z}{\partial \phi} - \frac{\partial H_\varphi}{\partial z} \tag{2}$$

$$\varepsilon \frac{\partial E_\varphi}{\partial t} = \frac{\partial H_\rho}{\partial z} - \frac{\partial H_z}{\partial \rho} \tag{3}$$

$$\varepsilon \frac{\partial E_z}{\partial t} = \frac{1}{\rho}\frac{\partial (\rho H_\varphi)}{\partial \rho} - \frac{1}{\rho}\frac{\partial H_\rho}{\partial \varphi} \tag{4}$$

Also for the sake of simplicity and without loss of generality, the electric and magnetic fields are expanded in terms of scaling functions only in space domain and pulse functions in time domain.

$$E_\rho(\mathbf{r}, t) = \sum_{i,j,k,n=-\infty}^{+\infty} E_{i+1/2,j,k}^{\phi\rho,n} h_n(t)\phi_{i+1/2}(\rho)\phi_j(\varphi)\phi_k(z) \tag{5}$$

$$E_\varphi(\mathbf{r}, t) = \sum_{i,j,k,n=-\infty}^{+\infty} E_{i,j+1/2,k}^{\phi\varphi,n} h_n(t)\phi_i(\rho)\phi_{j+1/2}(\varphi)\phi_k(z) \tag{6}$$

$$E_z(\mathbf{r}, t) = \sum_{i,j,k,n=-\infty}^{+\infty} E_{i,j,k+1/2}^{\phi z,n} h_n(t)\phi_i(\rho)\phi_j(\varphi)\phi_{k+1/2}(z) \tag{7}$$

where $E_{i,j,k}^{\phi\kappa,n}$ with $\kappa = \rho, \varphi, z$ are the coefficients for the fields expansions in terms of scaling functions. The indexes i, j, k and n are the discrete space and time indices related to the space and time coordinates via $\rho = i\Delta\rho$, $\varphi = j\Delta\varphi$, $z = k\Delta z$ and $t = n\Delta t$, where $\Delta\rho$, $\Delta\varphi$, Δz and Δt, represent the space and time discretization intervals in ρ-, φ-, z- and t-direction. The function $h(t)$ is defined as Haar's scaling function, and $\phi(v)$ is Daubechies' scaling function. Moreover, the functions of $h_n(t)$ and $\phi_m(v)$ are defined by

$$h_n(t) = h\left(\frac{t}{\Delta t} - n\right) \tag{8}$$

$$\phi_m(x) = \phi\left(\frac{v}{\Delta v} - m\right), \quad v = \rho, \varphi, z \tag{9}$$

Substituting (5)–(7) to (2)–(4) and applying Galerkin scheme and wavelet function as following:

$$\left\langle h_m(x), \frac{\partial h_{m'+1/2}(x)}{\partial x} \right\rangle = \delta_{m,m'} - \delta_{m,m'+1} \tag{10}$$

$$\langle \varphi_m(x), \varphi_{m'}(x) \rangle = \delta_{m,m'}\Delta x \tag{11}$$

$$\left\langle \varphi_m(x), \frac{\partial \varphi_{m'+1/2}(x)}{\partial x} \right\rangle = \sum_l a(l)\delta_{m+l,m'} \tag{12}$$

As remarked by mathematicians [20], the shifted Daubechies D_2 scaling functions has approximate sampling properties. Therefore (9) is modified to

$$\phi_i\left(\frac{x}{\Delta x} - i + M_1\right) = \delta_{k,0}, \tag{13}$$

where

$$M_1 = \int_{-\infty}^{+\infty} x\phi(x)dx$$

is the first-order moment of the scaling function and δ the Kronecker delta function. This property yields a simple algorithm for inhomogeneous problems through the local sampling of the field values regardless of the complexity of the inhomogeneity. The numerical values of the coefficients $\{a(l)\}$ have been tabulated in [16].

Take E_ρ as example, the component of which at point $((i+1/2)\Delta\rho, j\Delta\varphi, k\Delta z, n\Delta t)$ is given by

$$E_\rho\left((i+1/2)\Delta\rho, j\Delta\varphi, k\Delta z, n\Delta t\right) = \int_{-\infty}^{\infty}\int_{-\infty}^{\infty}\int_{-\infty}^{\infty}\int_{-\infty}^{\infty} E_\rho(r,t)\delta\left(\frac{\rho}{\Delta\rho}-i-\frac{1}{2}\right)$$
$$\cdot\delta\left(\frac{\varphi}{\Delta\varphi}-j\right)\delta\left(\frac{z}{\Delta z}-k\right)\delta\left(\frac{t}{\Delta t}-n\right)\rho d\rho d\varphi dz dt = E_{i+1/2,j,k}^{\phi\rho,n} \quad (14)$$

This equation related to the total electric value is the sampling value of this point, so we can obtain the MRTD equations based on Daubechies scaling function as following:

$$E_{i+1/2,j,k}^{\phi\rho,n+1} = E_{i+1/2,j,k}^{\phi\rho,n}$$
$$+\frac{\Delta t}{\varepsilon}\left[\frac{1}{(i+1/2)\Delta\rho\Delta\varphi}\sum_l a(l)H_{i+1/2,j+l+1/2,k}^{\phi z,n+1/2} - \frac{1}{\Delta z}\sum_l a(l)H_{i+1/2,j,k+l+1/2}^{\phi\varphi,n+1/2}\right] \quad (15)$$

$$E_{i,j+1/2,k}^{\phi\varphi,n+1} = E_{i,j+1/2,k}^{\phi\varphi,n}$$
$$+\frac{\Delta t}{\varepsilon}\left[\frac{1}{\Delta z}\sum_l a(l)H_{i,j+1/2,k+l+1/2}^{\phi\rho,n+1/2} - \frac{1}{\Delta\rho}\sum_l a(l)H_{i+l+1/2,j+1/2,k}^{\phi z,n+1/2}\right] \quad (16)$$

$$E_{i,j,k+1/2}^{\phi z,n+1} = E_{i,j,k+1/2}^{\phi z,n}$$
$$+\frac{\Delta t}{\varepsilon}\left[\frac{1}{i\Delta\rho}\sum_l a(l)(i+l+1/2)H_{i+l+1/2,j,k+1/2}^{\phi\varphi,n+1/2} - \frac{1}{i\Delta\rho\Delta\varphi}\sum_l a(l)H_{i,j+l+1/2,k+1/2}^{\phi\rho,n+1/2}\right] \quad (17)$$

The other set of equations for updating **H** field can be obtained by duality. The stability and dispersion analyses are available in [16], so it is not shown here for saving space.

2.2. CPML Scheme

In the CPML layer, the formulation is posed in the stretched coordinate space [21, 22]. For the sake of generality example, a lossy medium is assumed here, we take **E** field as example, the **H** field can be obtained by duality.

$$j\omega\varepsilon E_\rho + \sigma E_\rho = \frac{1}{\rho}\frac{\partial H_z}{s_\varphi\partial\varphi} - \frac{\partial H_\varphi}{s_z\partial z} \quad (18)$$

$$j\omega\varepsilon E_\varphi + \sigma E_\varphi = \frac{\partial H_\rho}{s_z\partial z} - \frac{\partial H_z}{s_\rho\partial\rho} \quad (19)$$

$$j\omega\varepsilon E_z + \sigma E_z = \frac{1}{\tilde{\rho}s_\rho}\frac{\partial(\tilde{\rho}H_\varphi)}{\partial\rho} - \frac{1}{\rho s_\varphi}\frac{\partial H_\rho}{\partial\varphi} \quad (20)$$

where s_i are the stretched-coordinate metric, which are proposed to be

$$s_i = \kappa_i + \frac{\sigma_i}{\alpha_i + j\omega\varepsilon_0}, \quad i = \rho, \varphi, z \quad (21)$$

where α_i, σ_i and κ_i are all assumed to be real and $\alpha_i > 0$, $\sigma_i > 0$, $\kappa_i \geq 1$, respectively. For simplicity, α is defined as constant through the CPML, and s_φ is chosen to be

$$s_\varphi = \frac{\tilde{\rho}}{\rho}$$

where $\tilde{\rho}$ can be defined as

$$\tilde{\rho} = \int_0^\rho s_\rho(\rho')d\rho' = \int_0^\rho\left[\kappa_\rho + \frac{\sigma(\rho')}{\alpha_\rho + j\omega\varepsilon_0}\right]d\rho' = \left(\kappa_\rho' + \frac{\sigma_\rho'}{\alpha_\rho + j\omega\varepsilon_0}\right)\rho = s_{\rho'} \quad (22)$$

Then the Eq. (20) can be rewritten as

$$j\omega\varepsilon E_z + \sigma E_z = \frac{H_\varphi}{\tilde{\rho}s_\rho}\frac{\partial\tilde{\rho}}{\partial\rho} + \frac{1}{s_\rho}\frac{\partial H_\varphi}{\partial\rho} - \frac{1}{\tilde{\rho}}\frac{\partial H_\rho}{\partial\varphi} = \frac{H_\varphi}{s_{\rho'}} + \frac{1}{s_\rho}\frac{\partial H_\varphi}{\partial\rho} - \frac{1}{s_{\rho'}}\frac{\partial H_\rho}{\partial\varphi} \quad (23)$$

Defining that $s'_i = s_i^{-1}$, we can get

$$s'_i = \frac{1}{\kappa_i} + \frac{\sigma'_i}{\alpha'_i + j\omega\varepsilon'_i}, \quad i = \rho, \varphi, z, \rho' \tag{24}$$

where $\sigma'_i = -\sigma_i$, $\varepsilon'_i = \varepsilon_0\kappa_i^2$ and $\alpha'_i = \kappa_i^2\alpha_i + \kappa_i\sigma_i$. Using Laplace transform theory, it can be obtained that s'_i has the impulse response

$$s'_i(t) = \frac{\delta(t)}{\kappa_i} + \frac{\sigma'_i}{\varepsilon'_i}e^{-\frac{\alpha'_i}{\varepsilon'_i}t}u(t) = \frac{\delta(t)}{\kappa_i} + \zeta_i(t) \tag{25}$$

where $\delta(t)$ is the unit impulse function and $u(t)$ the step function. Utilizing (25), Eqs. (18), (19) and (23) can transformed into time domain

$$\begin{aligned}
\varepsilon\frac{\partial}{\partial t}E_\rho(t) + \sigma E_\rho(t) &= \frac{1}{\rho}s'_\varphi(t) * \frac{\partial}{\partial\varphi}H_z(t) - s'_z * \frac{\partial}{\partial z}H_\varphi(t)\\
&= \frac{1}{\rho\kappa_\varphi}\frac{\partial}{\partial\varphi}H_z(t) - \frac{1}{\kappa_z}\frac{\partial}{\partial z}H_\varphi(t) + \int_0^t \frac{\partial}{\partial\varphi}H_z(t-\tau)\zeta_z(\tau)d\tau\\
&\quad - \int_0^t \frac{\partial}{\partial z}H_\varphi(t-\tau)\zeta_\varphi(\tau)d\tau
\end{aligned} \tag{26}$$

$$\begin{aligned}
\varepsilon\frac{\partial}{\partial t}E_\varphi(t) + \sigma E_\varphi(t) &= s'_z * \frac{\partial}{\partial z}H_\rho(t) - s'_\rho * \frac{\partial}{\partial\rho}H_z(t)\\
&= \frac{1}{\kappa_z}\frac{\partial}{\partial z}H_\rho(t) - \frac{1}{\kappa_\rho}\frac{\partial}{\partial\rho}H_z(t) + \int_0^t \frac{\partial}{\partial z}H_\rho(t-\tau)\zeta_\rho(\tau)d\tau\\
&\quad - \int_0^t \frac{\partial}{\partial\rho}H_z(t-\tau)\zeta_z(\tau)d\tau
\end{aligned} \tag{27}$$

$$\begin{aligned}
\varepsilon\frac{\partial}{\partial t}E_z(t) + \sigma E_z(t) &= s'_\rho * \frac{\partial}{\partial\rho}H_\varphi(t) + s'_{\rho'} * \left(H_\varphi - \frac{\partial}{\partial\varphi}H_\rho(t)\right)\\
&= \frac{1}{\kappa_\rho}\frac{\partial}{\partial\rho}H_\varphi(t) - \frac{1}{\kappa_{\rho'}}\frac{\partial}{\partial z}\left(H_\varphi(t) - \frac{\partial}{\partial\varphi}H_\rho(t)\right) + \int_0^t \frac{\partial}{\partial\rho}H_\varphi(t-\tau)\zeta_\varphi(\tau)d\tau\\
&\quad - \int_0^t \left(H_\varphi(t-\tau) - \frac{\partial}{\partial z}H_\rho(t-\tau)\right)\zeta_{\rho'}(\tau)d\tau
\end{aligned} \tag{28}$$

The discrete impulse response for $\zeta_i(t)$ can be defined as

$$S_i(m) = \int_{m\Delta t}^{(m+1)\Delta t} \zeta(\tau)d\tau = -\frac{\sigma_i}{\varepsilon_0\kappa_i^2}\int_{m\Delta t}^{(m+1)\Delta t} e^{-\left(\frac{\sigma_i}{\kappa_i\varepsilon_0} + \frac{\alpha_i}{\varepsilon_0}\right)\tau}d\tau = a_i e^{-\left(\frac{\sigma_i}{\kappa_i} + \alpha\right)_i \frac{m\Delta t}{\varepsilon_0}}, \tag{29}$$

where

$$a_i = \frac{\sigma_i}{\sigma_i\kappa_i + \kappa_i^2\alpha_i}\left(e^{-\left(\frac{\sigma_i}{\kappa_i} + \alpha_i\right)\frac{\Delta t}{\varepsilon_0}} - 1\right). \tag{30}$$

Then following the procedure of [17] and according to the wavelet-Galerkin scheme based on Daubechies' compactly supported wavelets, the MRTD equations for E_ρ, E_φ and E_z can be obtained as following:

$$\begin{aligned}
E_{i+\frac{1}{2},j,k}^{\phi\rho,n+1} &= CA_{i+\frac{1}{2},j,k}E_{i+\frac{1}{2},j,k}^{\phi\rho,n} + CB_{i+\frac{1}{2},j,k}\left[\frac{1}{\kappa'_\rho(i+1/2)\Delta\rho\Delta\varphi}\sum_l a(l)H_{i+\frac{1}{2},j+l+\frac{1}{2},k}^{\phi z,n+\frac{1}{2}}\right.\\
&\quad \left. -\frac{1}{\kappa_z\Delta z}\sum_l a(l)H_{i+\frac{1}{2},j,k+l+\frac{1}{2}}^{\phi\varphi,n+\frac{1}{2}}\right] + CB_{i+\frac{1}{2},j,k}\left(\psi_{e_{\rho\varphi},i+\frac{1}{2},j,k}^{\phi\rho,n+\frac{1}{2}} - \psi_{e_{\rho z},i+\frac{1}{2},j,k}^{\phi\rho,n+\frac{1}{2}}\right)
\end{aligned} \tag{31}$$

$$E_{i,j+\frac{1}{2},k}^{\phi\varphi,n+1} = CA_{i,j+\frac{1}{2},k}E_{i,j+\frac{1}{2},k}^{\phi\varphi,n} + CB_{i,j+\frac{1}{2},k}\left[\frac{1}{\kappa_z\Delta z}\sum_l a(l)H_{i,j+\frac{1}{2},k+l+\frac{1}{2}}^{\phi\rho,n+\frac{1}{2}}\right.$$

$$-\frac{1}{\kappa_\rho \Delta\rho}\sum_l a(l)H^{\phi z,n+\frac{1}{2}}_{i+\frac{1}{2},j+l+\frac{1}{2},k}\Bigg] + CB_{i,j+\frac{1}{2},k}\left(\psi^{\phi\varphi,n+\frac{1}{2}}_{e_{\varphi z},i,j+\frac{1}{2},k} - \psi^{\phi\varphi,n+\frac{1}{2}}_{e_{\varphi\rho},i,j+\frac{1}{2},k}\right) \tag{32}$$

$$\begin{aligned}
E^{\phi z,n+1}_{i,j,k+1/2} =\ & CA_{i,j,k+1/2}E^{\phi z,n}_{i,j,k+1/2} + CB_{i,j,k+1/2}\Bigg[\frac{1}{\kappa_\rho \Delta\rho}\sum_l a(l)H^{\phi\varphi,n+1/2}_{i+l+1/2,j,k+1/2}\\
& +\frac{1}{\kappa'_\rho i\Delta\rho}\left(\frac{H^{\phi\varphi,n+\frac{1}{2}}_{i+1/2,j,k+1/2} + H^{\phi\varphi,n-\frac{1}{2}}_{i+1/2,j,k+1/2}}{2} - \frac{1}{\Delta\varphi}\sum_l a(l)H^{\phi\rho,n+\frac{1}{2}}_{i,j+l+1/2,k+1/2}\right)\Bigg]\\
& + CB_{i,j,k+\frac{1}{2}}\left(\psi^{\phi z,n+1/2}_{e_{z\rho},i,j,k+1/2} + \psi^{\phi z,n+1/2}_{e_{z\varphi},i,j,k+1/2}\right)
\end{aligned} \tag{33}$$

where

$$\psi^{\phi\rho,n+\frac{1}{2}}_{e_{\rho\varphi},i+\frac{1}{2},j,k} = P'_\rho \psi^{\phi\rho,n-\frac{1}{2}}_{e_{\rho\varphi},i+\frac{1}{2},j,k} + Q'_\rho \sum_l a(l)\frac{H^{\phi z,n+\frac{1}{2}}_{i+\frac{1}{2},j+l+\frac{1}{2},k}}{(i+1/2)\,\Delta\rho\Delta\varphi} \tag{34}$$

$$\psi^{\phi x,n+\frac{1}{2}}_{e_{\rho z},i+\frac{1}{2},j,k} = P_z \psi^{\phi x,n-\frac{1}{2}}_{e_{\rho z},i+\frac{1}{2},j,k} + Q_z \sum_l a(l)\frac{H^{\phi\varphi,n+\frac{1}{2}}_{i+\frac{1}{2},j,k+l+\frac{1}{2}}}{\Delta z} \tag{35}$$

$$\psi^{\phi\varphi,n+1/2}_{e_{\varphi z},i,j+1/2,k} = P_z \psi^{\phi\varphi,n-1/2}_{e_{\varphi z},i,j+1/2,k} + Q_z \sum_l a(l)\frac{H^{\phi\rho,n+1/2}_{i,j+1/2,k+l+1/2}}{\Delta z} \tag{36}$$

$$\psi^{\phi\varphi,n+1/2}_{e_{\varphi\rho},i,j+1/2,k} = P_\rho \psi^{\phi\varphi,n-1/2}_{e_{\varphi\rho},i,j+1/2,k} + Q_\rho \sum_l a(l)\frac{H^{\phi z,n+1/2}_{i+l+1/2,j+1/2,k}}{\Delta\rho} \tag{37}$$

$$\psi^{\phi z,n+1/2}_{e_{z\rho},i,j,k+1/2} = P_\rho \psi^{\phi z,n-1/2}_{e_{z\rho},i,j,k+1/2} + Q_\rho \frac{1}{\Delta\rho}\sum_l a(l)H^{\phi\varphi,n+\frac{1}{2}}_{i+l+\frac{1}{2},j,k+\frac{1}{2}} \tag{38}$$

$$\begin{aligned}
\psi^{\phi z,n+1/2}_{e_{z\varphi},i,j,k+1/2} =\ & P'_\rho \psi^{\phi z,n-1/2}_{e_{z\varphi},i,j,k+1/2} + Q'_\rho \frac{1}{\kappa'_\rho i\Delta\rho}\\
& \times\left(\frac{H^{\phi\varphi,n+\frac{1}{2}}_{i+1/2,j,k+1/2} + H^{\phi\varphi,n-\frac{1}{2}}_{i+1/2,j,k+1/2}}{2} - \frac{1}{\Delta\varphi}\sum_l a(l)H^{\phi\rho,n+\frac{1}{2}}_{i,j+l+1/2,k+1/2}\right)
\end{aligned} \tag{39}$$

$$CA_{i,j,k} = \frac{2\varepsilon_{i,j,k} - \sigma_{i,j,k}\Delta t}{2\varepsilon_{i,j,k} + \sigma_{i,j,k}\Delta t}, \quad CB_{i,j,k} = \frac{2\Delta t}{2\varepsilon_{i,j,k} + \sigma_{i,j,k}\Delta t}$$

$$P'_\rho = e^{-\left(\frac{\sigma'_\rho}{\kappa'_\rho} + \alpha'_\rho\right)\frac{\Delta t}{\varepsilon_0}}, \quad Q'_\rho = \frac{\sigma'_\rho}{\sigma'_\rho \kappa'_\rho + \kappa'^2_\rho \alpha'_\rho}\left(e^{-\left(\frac{\sigma'_\rho}{\kappa'_\rho} + \alpha'_\rho\right)\frac{\Delta t}{\varepsilon_0}} - 1\right)$$

$$P_\xi = e^{-\left(\frac{\sigma_\xi}{\kappa_\xi} + \alpha_\xi\right)\frac{\Delta t}{\varepsilon_0}}, \quad Q_\xi = \frac{\sigma_\xi}{\sigma_\xi \kappa_\xi + \kappa^2_\xi \alpha_\xi}\left(e^{-\left(\frac{\sigma_\xi}{\kappa_\xi} + \alpha_\xi\right)\frac{\Delta t}{\varepsilon_0}} - 1\right), \quad \xi = \rho, \varphi, z$$

The other set of equations for updating **H** field can be obtained by duality.

2.3. QCPML Scheme

In Eqs. (18)–(20), if we define $\tilde{\rho} = \rho$ and $s_\varphi = 1$, the 3-D updating equations for **E** field in time-domain can be given by

$$\varepsilon\frac{\partial E_\rho}{\partial t} + \sigma E_\rho = \frac{1}{\rho}\frac{\partial}{\partial\varphi}H_z - \frac{1}{\kappa_z}\frac{\partial}{\partial z}H_\varphi - \psi_{e_{\rho z}} \tag{40}$$

$$\varepsilon \frac{\partial E_\varphi}{\partial t} + \sigma E_\varphi = \frac{\partial H_\rho}{\kappa_z \partial z} - \frac{\partial H_z}{\kappa_\rho \partial \rho} + \psi_{e_{\varphi z}} - \psi_{e_{\varphi \rho}} \tag{41}$$

$$\varepsilon \frac{\partial E_z}{\partial t} + \sigma E_z = \frac{1}{\rho s_\rho} \frac{\partial (\rho H_\varphi)}{\partial \rho} - \frac{1}{\rho} \frac{\partial H_\rho}{\partial \varphi} + \psi_{e_{z\rho}}. \tag{42}$$

Compared with the CPML formulations above, this system requires only 8 instead of 12 auxiliary variables in the 3-D case, which implies that it is more advantageous to save computation time and computer memory. Since it is not theoretically a perfect matched layer, thus it is named Quasi-CPML, or simply QCPML. The discretization scheme of Eqs. (40)–(42) can follow Eqs. (31)–(39).

2.4. Berenger's PML Scheme

Here we also take **E** field as example. Following the procedure of [16], the equations for the PML in a lossy medium can be obtained as

$$\varepsilon \frac{\partial E_{\rho\varphi}}{\partial t} + \left(\sigma + \varepsilon_r \sigma_{E'}^\rho \right) E_{\rho\varphi} + \xi_{\rho\varphi} = \frac{1}{\rho} \frac{\partial (H_{z\rho} + H_{z\varphi})}{\partial \phi} \tag{43}$$

$$\varepsilon \frac{\partial E_{\rho z}}{\partial t} + \left(\sigma + \varepsilon_r \sigma_E^z \right) E_{\rho z} + \xi_{\rho z} = -\frac{\partial (H_{\varphi z} + H_{\varphi \rho})}{\partial z} \tag{44}$$

$$\varepsilon \frac{\partial E_{\varphi z}}{\partial t} + \left(\sigma + \varepsilon_r \sigma_E^z \right) E_{\varphi z} + \xi_{\varphi z} = \frac{\partial (H_{\rho\varphi} + H_{\rho z})}{\partial z} \tag{45}$$

$$\varepsilon \frac{\partial E_{\varphi\rho}}{\partial t} + \left(\sigma + \varepsilon_r \sigma_E^\rho \right) E_{\varphi\rho} + \xi_{\varphi\rho} = -\frac{\partial (H_{z\rho} + H_{z\varphi})}{\partial \rho} \tag{46}$$

$$\varepsilon \frac{\partial E_{z\rho}}{\partial t} + \left(\sigma + \varepsilon_r \sigma_E^\rho \right) E_{z\rho} + \xi_{z\rho} = \frac{\partial H_\varphi}{\partial \rho} \tag{47}$$

$$\varepsilon \frac{\partial E_{z\varphi}}{\partial t} + \left(\sigma + \varepsilon_r \sigma_{E'}^\rho \right) E_{z\varphi} + \xi_{z\varphi} = \frac{1}{\rho} \left(H_\varphi - \frac{\partial H_\rho}{\partial \varphi} \right) \tag{48}$$

where

$$\frac{\partial \xi_{\rho\varphi}}{\partial t} = \frac{\sigma \sigma_{E'}^\rho}{\varepsilon_0} E_{\rho\varphi}, \quad \frac{\partial \xi_{\rho z}}{\partial t} = \frac{\sigma \sigma_E^z}{\varepsilon_0} E_{\rho z}$$

$$\frac{\partial \xi_{\varphi z}}{\partial t} = \frac{\sigma \sigma_E^z}{\varepsilon_0} E_{\varphi z}, \quad \frac{\partial \xi_{\varphi\rho}}{\partial t} = \frac{\sigma \sigma_E^\rho}{\varepsilon_0} E_{\varphi\rho}$$

$$\frac{\partial \xi_{z\rho}}{\partial t} = \frac{\sigma \sigma_E^\rho}{\varepsilon_0} E_{z\rho}, \quad \frac{\partial \xi_{z\varphi}}{\partial t} = \frac{\sigma \sigma_{E'}^\rho}{\varepsilon_0} E_{z\varphi}$$

where the definitions of $\sigma_{E'}^\rho$, σ_E^ρ and σ_E^z are available in [16]. And the split PML equations can be written as

$$E_{i+1/2,j,k}^{\phi\rho\varphi,n+1} = \exp\left(- \left(\kappa'_{i+1/2}\sigma + \varepsilon_r \sigma_{E'}^{i+1/2} \right) \Delta t / \kappa'_i \varepsilon \right) E_{i+1/2,j,k}^{\phi\rho\varphi,n}$$

$$+ \frac{1 - \exp\left(- \left(\kappa'_{i+1/2}\sigma + \varepsilon_r \sigma_{E'}^{i+1/2} \right) \Delta t / \kappa'_{i+1/2} \varepsilon \right)}{\left(\kappa'_{i+1/2}\sigma + \varepsilon_r \sigma_{E'}^{i+1/2} \right)}$$

$$\times \left[\frac{1}{(i+1/2) \Delta\rho \Delta\varphi} \sum_l a(l) H_{i+1/2,j+l+1/2,k}^{\phi z,n+1/2} - \xi_{\rho\varphi,i+1/2,j,k}^{n+1/2} \right] \tag{49}$$

$$E_{i+1/2,j,k}^{\phi\rho z,n+1} = \exp\left(- \left(\kappa_k \sigma + \varepsilon_r \sigma_E^k \right) \Delta t / \kappa_k \varepsilon \right) E_{i+1/2,j,k}^{\phi\rho z,n}$$

$$- \frac{1 - \exp\left(- \left(\kappa_k \sigma + \varepsilon_r \sigma_E^k \right) \Delta t / \kappa_k \varepsilon \right)}{\left(\kappa_k \sigma + \varepsilon_r \sigma_E^k \right)}$$

$$\times \sum_l a(l) \left[\frac{1}{\Delta z} H_{i+1/2,j,k+l+1/2}^{\phi\varphi,n+1/2} - \xi_{\rho z,i+1/2,j,k}^{n+1/2} \right] \tag{50}$$

$$
\begin{aligned}
E_{i,j+1/2,k}^{\phi\varphi z,n+1} &= \exp\left(-\left(\kappa_k\sigma + \varepsilon_r\sigma_E^k\right)\Delta t/\kappa_k\varepsilon\right)E_{i,j+1/2,k}^{\phi\varphi z,n} \\
&\quad + \frac{1-\exp\left(-\left(\kappa_k\sigma + \varepsilon_r\sigma_E^k\right)\Delta t/\kappa_k\varepsilon\right)}{\left(\kappa_k\sigma + \varepsilon_r\sigma_E^k\right)} \\
&\quad \times \left[\frac{1}{\Delta z}\sum_l a\left(l\right)H_{i,j+1/2}^{\phi\rho,n+1/2} - \xi_{\varphi z,i,j+1/2,k}^{n+1/2}\right]
\end{aligned} \tag{51}
$$

$$
\begin{aligned}
E_{i,j+1/2,k}^{\phi\varphi\rho,n+1} &= \exp\left(-\left(\kappa_i\sigma + \varepsilon_r\sigma_E^i\right)\Delta t/\kappa_i\varepsilon\right)E_{i,j+1/2,k}^{\phi\varphi\rho,n} \\
&\quad - \frac{1-\exp\left(-\left(\kappa_i\sigma + \varepsilon_r\sigma_E^i\right)\Delta t/\kappa_i\varepsilon\right)}{\left(\kappa_i\sigma + \varepsilon_r\sigma_E^i\right)} \\
&\quad \times \left[\frac{1}{\Delta\rho}\sum_l a\left(l\right)H_{i+l+1/2,j+1/2,k}^{\phi z,n+1/2} - \xi_{\varphi\rho,i,j+1/2,k}^{n+1/2}\right]
\end{aligned} \tag{52}
$$

$$
\begin{aligned}
E_{i,j,k+1/2}^{\phi z\rho,n+1} &= \exp\left(-\left(\kappa_i\sigma + \varepsilon_r\sigma_E^i\right)\Delta t/\kappa_i\varepsilon\right)E_{i,j,k+1/2}^{\phi z\rho,n} \\
&\quad + \frac{1-\exp\left(-\left(\kappa_i\sigma + \varepsilon_r\sigma_E^i\right)\Delta t/\kappa_i\varepsilon\right)}{\left(\kappa_i\sigma + \varepsilon_r\sigma_E^i\right)} \\
&\quad \times \left[\frac{1}{\Delta\rho}\sum_l a\left(l\right)H_{i+l+1/2,j,k+1/2}^{\phi\varphi,n+1/2} - \xi_{z\rho,i,j,k+1/2}^{n+1/2}\right]
\end{aligned} \tag{53}
$$

$$
\begin{aligned}
E_{i,j,k+1/2}^{\phi z\varphi,n+1} &= \exp\left(-\left(\kappa_i'\sigma + \varepsilon_r\sigma_{E'}^i\right)\Delta t/\kappa'\varepsilon\right)E_{i,j,k+1/2}^{\phi z\varphi,n} \\
&\quad + \frac{1-\exp\left(-\left(\kappa_i'\sigma + \varepsilon_r\sigma_{E'}^i\right)\Delta t/\kappa'\varepsilon\right)}{\left(\kappa_i'\sigma + \varepsilon_r\sigma_{E'}^i\right)} \times \left[\frac{H_{i+1/2,j,k+1/2}^{\phi\varphi,n+1/2} + H_{i+1/2,j,k+1/2}^{\phi\varphi,n-1/2}}{2i\Delta\rho}\right. \\
&\quad \left. -\frac{1}{i\Delta\rho\Delta\varphi}\sum_l a\left(l\right)H_{i,j+l+1/2,k+1/2}^{\phi\rho,n+1/2} - \xi_{z\varphi,i,j,k+1/2}^{n+1/2}\right]
\end{aligned} \tag{54}
$$

where

$$
\xi_{\rho\varphi,i+1/2,j,k}^{n+1/2} = \xi_{\rho\varphi,i+1/2,j,k}^{n-1/2} + \frac{\sigma\sigma_{E'}^i\Delta t}{\varepsilon_0}\left(\frac{E_{i+1/2,j,k}^{\phi\rho\varphi,n} + E_{i+1/2,j,k}^{\phi\rho\varphi,n-1}}{2}\right) \tag{55}
$$

$$
\xi_{\rho z,i+1/2,j,k}^{n+1/2} = \xi_{\rho z,i+1/2,j,k}^{n-1/2} + \frac{\sigma\sigma_E^k\Delta t}{\varepsilon_0}\left(\frac{E_{i+1/2,j,k}^{\phi\rho z,n} + E_{i+1/2,j,k}^{\phi\rho z,n-1}}{2}\right) \tag{56}
$$

$$
\xi_{\varphi z,i,j+1/2,k}^{n+1/2} = \xi_{\varphi z,i,j+1/2,k}^{n-1/2} + \frac{\sigma\sigma_E^k\Delta t}{\varepsilon_0}\left(\frac{E_{i,j+1/2,k}^{\phi\varphi z,n} + E_{i,j+1/2,k}^{\phi\varphi z,n-1}}{2}\right) \tag{57}
$$

$$
\xi_{\varphi\rho,i,j+1/2,k}^{n+1/2} = \xi_{\varphi\rho,i,j+1/2,k}^{n-1/2} + \frac{\sigma\sigma_E^i\Delta t}{\varepsilon_0}\left(\frac{E_{i,j+1/2,k}^{\phi\varphi\rho,n} + E_{i,j+1/2,k}^{\phi\varphi\rho,n-1}}{2}\right) \tag{58}
$$

$$
\xi_{z\rho,i,j,k+1/2}^{n+1/2} = \xi_{z\rho,i,j,k+1/2}^{n-1/2} + \frac{\sigma\sigma_E^i\Delta t}{\varepsilon_0}\left(\frac{E_{i,j,k+1/2}^{\phi z\rho,n} + E_{i,j,k+1/2}^{\phi z\rho,n-1}}{2}\right) \tag{59}
$$

$$
\xi_{z\varphi,i,j,k+1/2}^{n+1/2} = \xi_{z\varphi,i,j,k+1/2}^{n-1/2} + \frac{\sigma\sigma_{E'}^i\Delta t}{\varepsilon_0}\left(\frac{E_{i,j,k+1/2}^{\phi z\varphi,n} + E_{i,j,k+1/2}^{\phi z\varphi,n-1}}{2}\right) \tag{60}
$$

The other set of equations for updating **H** field can be obtained by duality.

3. NUMERICAL RESULTS

3.1. Validation of Convergence

In this section, we simulate a 3-D cylindrical case in the media with constitutive parameters $\varepsilon_r = 3.0$, $\sigma = 0.01$ to validate the convergence of both CPML and QCPML methods. The computation domain is discretized using a $(N_\rho, N_\varphi, N_z) = (28, 30, 36)$ cell lattice with eight-cell-thick CPML and QCPML terminate the grid in ρ and z directions. Within the ABC's layer, the constitutive parameters σ_i and κ_i are scaled using an mth order polynomial scaling [23]

$$\sigma(d) = \sigma_{\max} \left(\frac{d}{D_{\mathrm{pml}}} \right)^m \tag{61}$$

$$\kappa(d) = 1 + (\kappa_{\max} - 1) \left(\frac{d}{D_{\mathrm{pml}}} \right)^m \tag{62}$$

where d denotes the distance from the computational-space/PML interface into the PML layer, D_{pml} is the depth of the PML, and m is the order of the polynomial. The choice for $\sigma_{\max}$ can be expressed as

$$\sigma_{\max} = k\sigma_{\mathrm{opt}} \tag{63}$$

$$\sigma_{\mathrm{opt}} = \frac{(m+1)}{150\pi\sqrt{\varepsilon_r}\Delta} \tag{64}$$

where $k = \sigma_{\max}/\sigma_{\mathrm{opt}}$ is nonnegative and real value. Here the designated parameters $\alpha = 0.01$, $\kappa_{\max} = 7$ and $\sigma_i = 0.5\sigma_{\mathrm{opt}}$. CPML and QCPML regions are terminated with a perfect electric conductor (PEC) wall [2, 16]. The cell discretization size is uniform in the ρ and z directions $\Delta\rho = \Delta z = 5$ cm. The source is a Gaussian pulse applied to the electric field component E_z located at the grid point (3, 0, 15) as follows:

$$E^{\phi z, n+1}_{3,0,15+1/2} = E^{\phi z, n}_{3,0,15+1/2} - E_0 \exp\left[-4\pi \left(n\Delta t - t_0\right)/\tau\right]^2 \tag{65}$$

where $\tau = 2.0$ ns, $t_0 = 0.8\tau$ and $E_0 = 1000$ V/m. The receiver is located at the grid point (18, 10, 21). From Fig. 1 the agreement between analytical curve and the numerical results of the CPML and QCPML schemes is evident, and we can see little reflection from the CPML and QCPML region. Any differences between the analytical and numerical solutions may be attributed to modelling errors such as the discrete approximation or reflections due to imperfections at the CPML and QCPML. Note that the source-receiver positioning is such that the pulse passes through the $\rho = 0$ axis. This also verifies the accuracy and stability of the cylindrical MRTD algorithm in our discretization scheme.
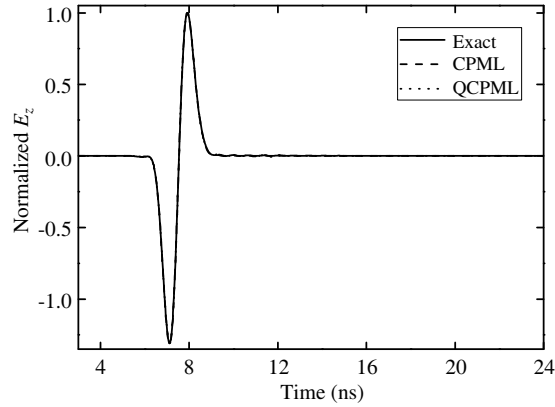

Figure 1. Comparison between analytical and numerical results for the CPML and QCPML schemes in cylindrical coordinates.

3.2. Reflection Error Analysis

In this section, we also simulate a 3-D cylindrical case in the media with constitutive parameters $\varepsilon_r = 3.0$ and $\sigma = 0.01$. Since there is a need to work with a PML of finite thickness and because of the discretization process, the CPML and QCPML are not reflectionless, and a small spurious reflection is present. In order to investigate the amount of spurious reflection caused by the discrete CPML and QCPML, two cylindrical MRTD grids are used: a test domain and a benchmark domain. The test domain is discretized using a $(N_\rho, N_\varphi, N_z) = (30, 30, 40)$ grid with ten-cell-thick CPML and QCPML terminate the grid in ρ and z directions, and the benchmark domain has untreated boundaries but a much larger size to isolate the error due to the CPML and QCPML. In this work, a cylindrical wave is applied to the electric field component E_φ as follows:

$$E^{\phi\varphi,n+1}_{3,1/2:N_\varphi-1/2,N_z/2-3:N_z/2+3} = E^{\phi\varphi,n}_{3,1/2:N_\varphi-1/2,N_z/2-3:N_z/2+3} - E_0 \exp\left[-4\pi\left(n\Delta t - t_0\right)/\tau\right]^2 \quad (66)$$

where $\tau = 6.0\,\mathrm{ns}$, $t_0 = 0.8\tau$ and $E_0 = 1000\,\mathrm{V/m}$. The receiver is located at the grid point $(10, 9, N_z/2)$. The cell discretization size is uniform in the ρ and z directions $\Delta\rho = \Delta z = 15\,\mathrm{cm}$, and the time step is chosen as $\Delta t = 38.856\,\mathrm{ps}$. The reflection error can be defined as

$$\mathrm{error_{dB}} = 20\log_{10}\frac{\left|E_\varphi(t) - E_{\varphi_{ref}}(t)\right|}{\max\left|E_{\varphi_{ref}}(t)\right|} \quad (67)$$

where $E_\varphi(t)$ represents the time-dependent discrete field computed within the test domain, $E_{\varphi_{ref}}(t)$ represents the same discrete field computed in the benchmark domain.

First, it is instructive to observe the maximum reflection errors incurred by the CPML and QCPML as a function of the constitutive parameters $\kappa_{\max}$, $\sigma_{\max}$ and α. Fig. 2(a) and Fig. 2(b) show the contour plots of the maximum relative error over 2000 time steps versus $\kappa_{\max}$ and $\sigma_{\max}$ with $\alpha = 0.01$ and $m = 4$ for the CPML and QCPML. It can be seen that the $-77\,\mathrm{dB}$ maximum error is achieved for the CPML, and $-87\,\mathrm{dB}$ for the QCPML. Compared with the QCPML, the optimal error for the CPML is realized over a much broader range of $\kappa_{\max}$ and $\sigma_{\max}$, but an improvement of $10\,\mathrm{dB}$ is obtained with the QCPML.
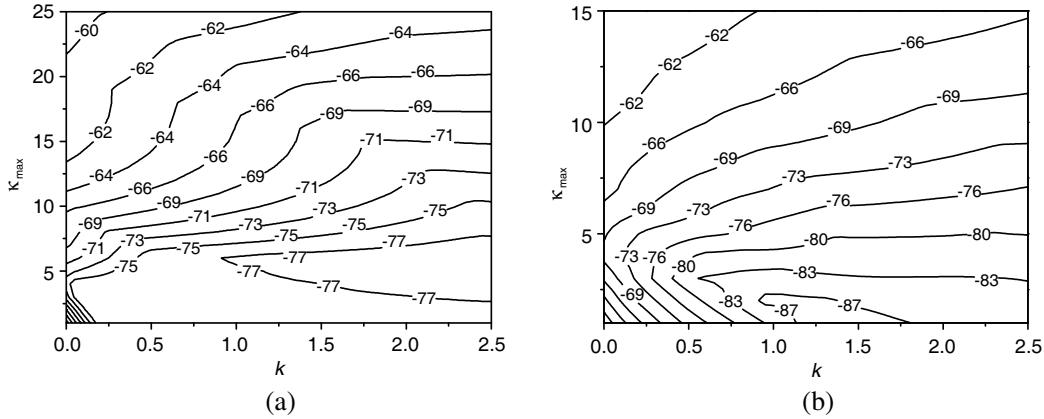

Figure 2. Contour plots of the maximum relative error for the first 2000 time steps. (a) CPML. (b) QCPML.

Figure 3(a) and Fig. 3(b) display the contour plots of the maximum relative error over 2000 time steps versus $\kappa_{\max}$ and α with $k = 1.4$ for the CPML and $k = 1.2$ for the QCPML. It can also be seen that the $-77\,\mathrm{dB}$ maximum error is achieved for the CPML, and $-87\,\mathrm{dB}$ for the QCPML. The optimal error for the CPML is realized over a much broader range of $\kappa_{\max}$ and α than the QCPML, but an improvement of $10\,\mathrm{dB}$ is obtained with the QCPML.

Figure 4(a) and Fig. 4(b) plot the contour plots of the maximum relative error over 2000 time steps versus α and $\sigma_{\max}$ with $\kappa_{\max} = 6$ for the CPML and $\kappa_{\max} = 2$ for the QCPML. And the conclusion is similar as before: the $-77\,\mathrm{dB}$ maximum error is achieved for the CPML, and $-87\,\mathrm{dB}$ for the QCPML;
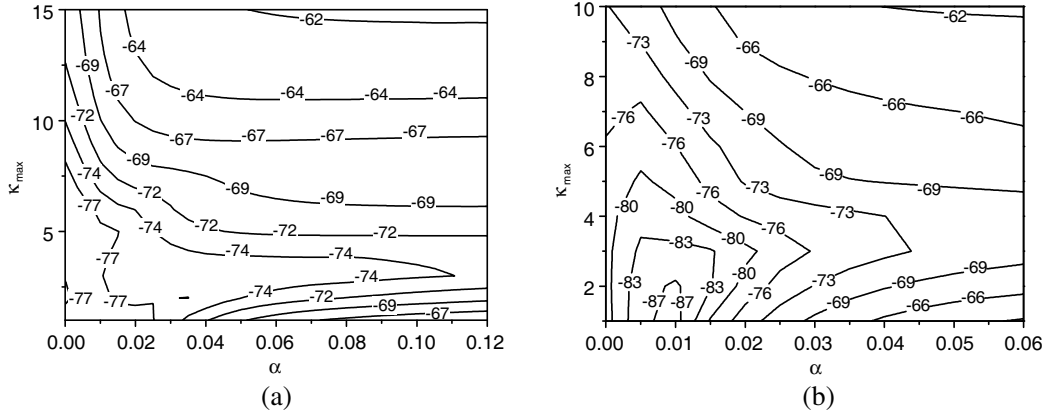
Figure 3. Contour plots of the maximum relative error for the first 2000 time steps. (a) CPML. (b) QCPML.
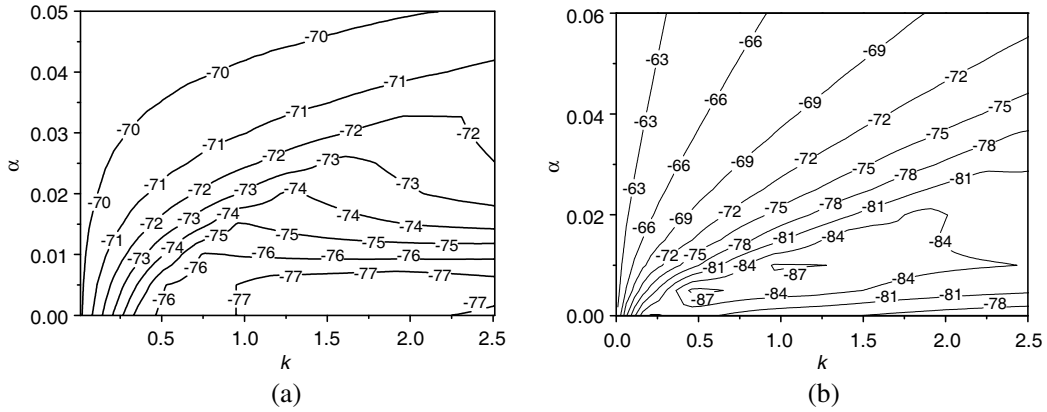

Figure 4. Contour plots of the maximum relative error for the first 2000 time steps. (a) CPML. (b) QCPML.

the optimal error for the CPML is realized over a much broader range of α and $\sigma_{\max}$, but an improvement of 10 dB is obtained with the QCPML.

Next, the reflection errors are studied for the CPML and QCPML. As illustrated in Fig. 5(a) and Fig. 5(b), the reflection errors as a function of N_{CPML} and N_{QCPML} are recorded, respectively. Here we define $\kappa_{\max} = 5$, $k = 1.4$, $\alpha = 0.005$ and $m = 4$ for the CPML method, and $\kappa_{\max} = 2$, $k = 1.2$, $\alpha = 0.005$, $m = 4$ for the QCPML method. It is seen that as N_{CPML} increases, the maximum reflection error has not reduced gradually, which is about on the order of -77 dB when $N_{\text{CPML}} \geq 8$ for the CPML method, and in the late time, the CPML method can provide a satisfying reflection error when $N_{\text{CPML}} \geq 8$. For the QCPML method, as N_{QCPML} increases, the maximum reflection error becomes smaller and smaller, which is less than -80 dB when $N_{\text{QCPML}} \geq 8$, and in the late time, the QCPML method can also provide a satisfying reflection error when $N_{\text{QCPML}} \geq 8$.

Figure 6(a) and Fig. 6(b) show the reflection errors as a function of the polynomial order m for the CPML and QCPML methods. Here we define $\kappa_{\max} = 5$, $k = 1.4$, $\alpha = 0.005$ and $N_{\text{CPML}} = 10$ for the CPML method, and $\kappa_{\max} = 2$, $k = 1.2$, $\alpha = 0.005$, $N_{\text{QCPML}} = 10$ for the QCPML method. From Fig. 6(a), it can be obtained that when $m \geq 2$, the maximum reflection error for the CPML is about on the order of -77 dB, and the absorbing effectiveness of CPML is satisfactory. Form Fig. 6(b), we can see that for the QCPML method, when $m \leq 4$, the maximum reflection error becomes smaller and smaller as m increases, which is about on the order of -87 dB when $m \geq 4$, and a satisfying reflection error can be obtained when $m \geq 3$.
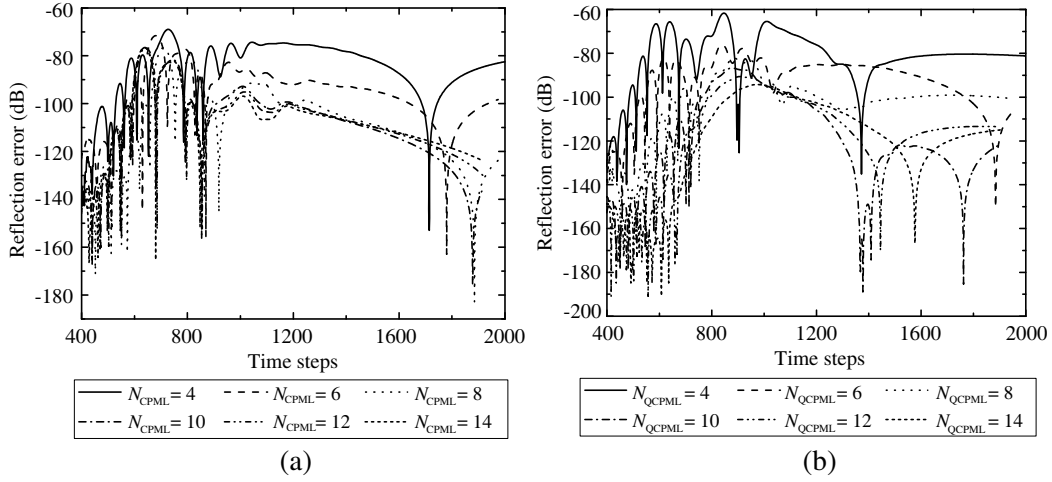
Figure 5. Local reflection error within test grid observed over the first 2000 time steps. (a) CPML. (b) QCPML.
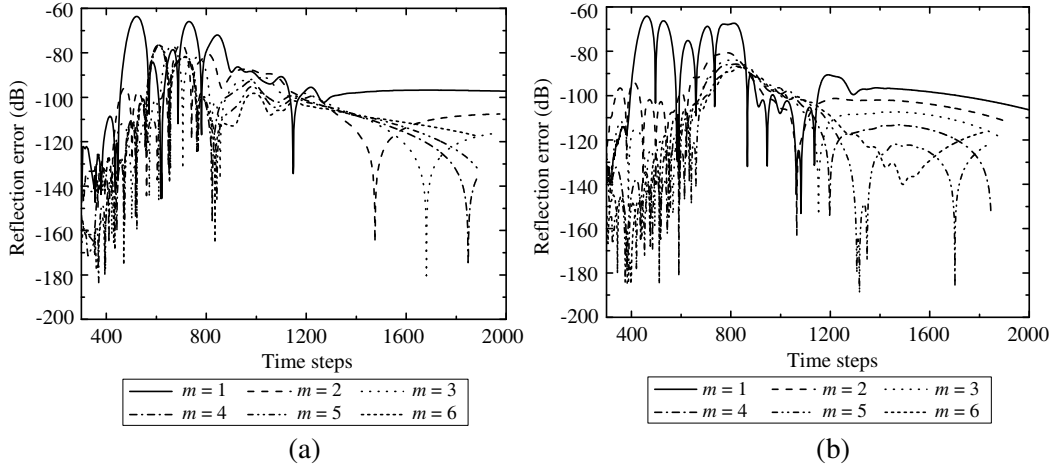

Figure 6. Local reflection error within test grid observed over the first 2000 time steps. (a) CPML. (b) QCPML.

Then the comparison of the reflection errors between the Berenger's PML, CPML and QCPML schemes is studied. The computational model is the same as before. For Berneger's PML, $\sigma_E^i = -\frac{\varepsilon_0 c(m+1)}{2D_{\mathrm{pml}}} \left|\frac{i}{D_{\mathrm{pml}}}\right|^m \ln[R(0)]$, $i = \rho, z$, here we define that $m = 4$, $R(0) = 10^{-4}$; for the CPML method, we define that $\kappa_{\max} = 5$, $k = 1.4$, $\alpha = 0.005$, $N_{\mathrm{CPML}} = 10$ and $m = 4$; for the QCPML method, $\kappa_{\max} = 2$, $k = 1.2$, $\alpha = 0.005$, $N_{\mathrm{QCPML}} = 10$ and $m = 5$. As illustrated in Fig. 7, the reflection error computed via (67) for each method is recorded. It is seen that no matter in the early or late time, the error caused by the PML is obviously more than that caused by the CPML or QCPML, and the QCPML has an advantage over the CPML.

In order to investigate the effectiveness of the CPML and QCPML at absorbing evanescent waves, a 3-D lattice of the dimension $20 \times 30 \times 40$ is used, surrounding a computation domain of the dimension $10 \times 30 \times 20$ with a PML layer 10-cell thick. Specifically, a $5 \times 30 \times 10$ PEC is immersed in a background media with constitutive parameters $\varepsilon_r = 3.0$ and $\sigma = 0.01$, as illustrated in Fig. 8. The excitation is applied to the electric field component E_φ at point A $(8, 12, 0)$ as follows

$$E_{8,1/2,12}^{\phi\varphi,n+1} = E_{8,1/2,12}^{\phi\varphi,n} - E_0 \exp\left[-4\pi\left(n\Delta t - t_0\right)/\tau\right]^2 \tag{68}$$
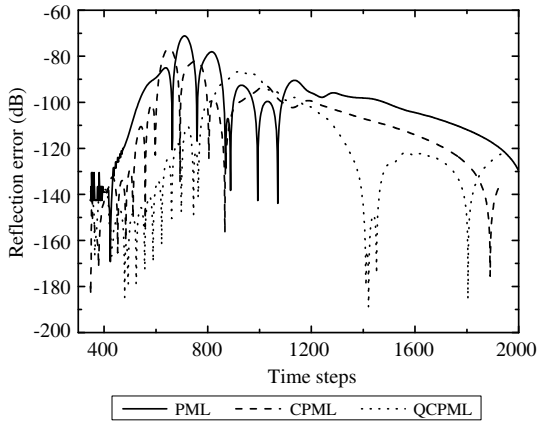
Figure 7. Comparison of the reflection errors between the Berenger's PML, CPML and QCPML.
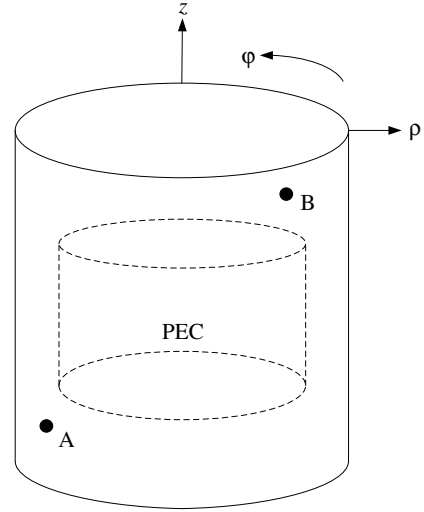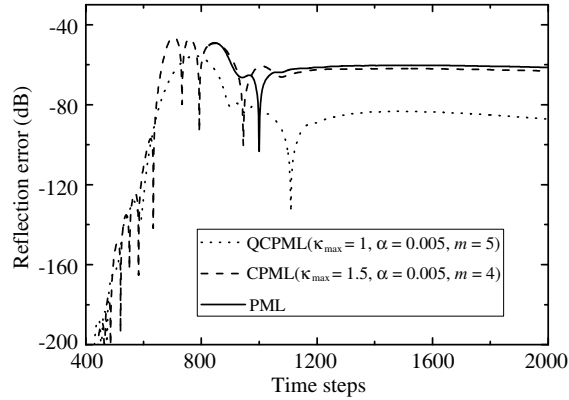

Figure 8. Computational model.

Figure 9. Comparison of the reflection errors between the Berenger's PML, CPML and QCPML.

where τ, t_0 and E_0 are the same as before. The receiver is located at point B (8, 20, 28). The cell discretization and the time step are also the same as before.

As illustrated in Fig. 9, the reflection error computed via (67) for each method is recorded. It is seen that in the late time, the error caused by the PML or CPML is obviously more than that caused by the QCPML, which demonstrate that the QCPML is more effective at absorbing the evanescent waves.

3.3. Comparison of the CPU Time and Memory between the PML, CPML and QCPML Schemes

In this section, the computation domain is discretized using a $30 \times 30 \times 60$ cell lattice with twenty-cell-thick PML, CPML and QCPML terminate the grid in ρ and z directions, the media in the computation domain and the designated parameters α, κ_i and σ_i are the same as before. Here the hard ware platform of the PC is as follows: Intel(R) Core(TM) i3 2.93 GHz CPU, 1.93 GB Memory; and the software platform: Microsoft Windows XP Professional, Fortran 90 Complier. As Table 1 shows, it is obvious that both the CPML and QCPML, especially the QCPML, have an advantage over PML at saving the CPU time and memory.

Table 1. CPU time and memory for PML and QPML.

Schemes	PML	CPML	QPML
CPU time/s ($5000\Delta t$)	117.531	88.094	68.125
CPU memory/MB	11.59	7.97	6.39

4. CONCLUSION

The CPML and QCPML absorbing boundary conditions are derived for cylindrical MRTD method. The implementation of both CPML and QCPML is independent of the host material, which implies that the CPML and QCPML formulations are unchanged in generalized media. The accuracy of the formulations is validated by computing the convergence. It is shown that the absorbing performance for both CPML and QCPML is satisfying and better than that of the PML, while the QCPML algorithm is more effective at absorbing the evanescent waves, and requires less CPU time and memory than PML and CPML.

ACKNOWLEDGMENT

REFERENCES

1. Krumpholz, M. and L. P. B. Katehi, "New prospects for time domain analysis," *IEEE Microwave Guided Wave Lett.*, Vol. 5, No. 11, 382–384, Dec. 1995.

2. Krumpholz, M. and L. P. B. Katehi, "MRTD: New time-domain schemes based on multiresolution analysis," *IEEE Trans. Microwave Theory Tech.*, Vol. 44, No. 4, 555–561, Apr. 1996.

3. Pan, G., M. V. Toupikov, and B. K. Gilbert, "On the use of Coifman intervallic wavelets in the method of moments for fast construction of wavelets sparsified matrices," *IEEE Trans. Antennas Propagat.*, Vol. 47, No. 7, 1189–1200, Jul. 1999.

4. Cheong, Y. W., Y. M. Lee, K. H. Ra, J. G. Kang, and C. C. Shin, "Wavelet-Galerkin scheme of time-dependent inhomogeneous electromagnetic problems," *IEEE Microwave Guided Wave Lett.*, Vol. 9, No. 8, 297–299, Aug. 1999.

5. Grivet-Talocia, S., "On the accuracy of Haar-based multiresolution time-domain schemes," *IEEE Microwave Wave Lett.*, Vol. 10, No. 10, 397–399, Oct. 2000.

6. Dogaru, T. and L. Carin, "Multiresolution time-domain using CDF biorthogonal wavelets," *IEEE Trans. Antennas Propagat.*, Vol. 49, No. 5, 902–912, May 2001.

7. Fujii, M. and W J. R. Hoefer, "Dispersion of time domain wavelet Galerkin method based on Daubechies' compactly supported scaling functions with three and four vanishing moments," *IEEE Microwave Guided Wave Lett.*, Vol. 10, No. 4, 125–127, Apr. 2000.

8. Kong, L.-Y., J. Wang, and W.-Y. Yin, "A novel dielectric conformal FDTD method for computing SAR distribution of the human body in a metallic cabin illuminated by an intentional electromagnetic pulse (IEMP)," *Progress In Electromagnetics Research*, Vol. 126, 355–373, 2012.

9. Mao, Y., B. Chen, H.-Q. Liu, J.-L. Xia, and J.-Z. Tang, "A hybrid implicit-explicit spectral FDTD scheme for oblique incidence problems on periodic structures," *Progress In Electromagnetics Research*, Vol. 128, 153–170, 2012.

10. Wang, J.-B., B.-H. Zhou, L.-H. Shi, C. Gao, and B. Chen, "A novel 3-D weakly conditionally stable FDTD algorithm," *Progress In Electromagnetics Research*, Vol. 130, 525–540, 2012.

11. Xiong, R., B. Chen, Y. Mao, B. Li, and Q.-F. Jing, "A simple local approximation FDTD model of short apertures with a finite thickness," *Progress In Electromagnetics Research*, Vol. 131, 135–152, 2012.

12. Xiong, R., B. Chen, J.-J. Han, Y.-Y. Qiu, W. Yang, and Q. Ning, "Transient resistance analysis of large grounding systems using the FDTD method," *Progress In Electromagnetics Research*, Vol. 132, 159–175, 2012.

13. Gradoni, G., V. Mariani Primiani, and F. Moglie, "Reverberation chamber as a multivariate process: FDTD evaluation of correlation matrix and independent positions," *Progress In Electromagnetics Research*, Vol. 133, 217–234, 2013.

14. Kong, Y.-D., Q.-X. Chu, and R.-L. Li, "High-order unconditionally-stable four-step adi-FDTD methods and numerical analysis," *Progress In Electromagnetics Research*, Vol. 135, 713–734, 2013.

15. Chun, K., H. Kim, H. Kim, and Y. Chung, "PLRC and ADE implementations of Drude-critical point dispersive model for the FDTD method," *Progress In Electromagnetics Research*, Vol. 135, 373–390, 2013.

16. Liu, Y., Y. Chen, B. Chen, and X. Xu, "A cylindrical MRTD algorithm with PML and quasi-PML," *IEEE Trans. Microwave Theory Tech.*, Vol. 61, No. 3, 1006–1017, Mar. 2013.

17. Roden, J. A. and S. D. Gedney, "Convolution PML (CPML): An efficient FDTD implementation of the CFS-PML for arbitrary media," *Microwave Opt. Technol. Lett.*, Vol. 27, No. 5, 334–339, Dec. 2000.

18. Abarbanel, S., D. Gottlieb, and J. S. Hesthaven, "Long time behavior of the perfectly matched layer equations in computational electromagnetics," *Journal of Scientific Computing*, Vol. 17, No. 1–4, 405–422, 2002.

19. Sweldens, W. and R. Piessens, "Wavelet sampling techniques," *Proc. Statistical Computing Section*, 20–29, 1993.

20. Berenger, J. P., "A perfectly matched layer for the absorption of electromagnetic waves," *J. Comput. Phys.*, Vol. 114, No. 2, 195–200, 1994.

21. Teixeira, F. L. and W. C. Chew, "PML-FDTD in cylindrical and spherical grids," *IEEE Microwave Guided Wave Lett.*, Vol. 7, No. 9, 285–287, Sep. 1997.

22. Chew, W. C. and W. H. Weedon, "A 3D perfectly matched medium from modified Maxwell's equations with stretched coordinates," *Microwave Opt. Technol. Lett.*, Vol. 7, No. 7, 599–604, Sep. 1994.

23. Gedney, S. D., "The perfectly matched layer absorbing medium," *Advances in Computational Electrodynamics: The Finite Difference Time Domain*, A. Taflove (ed.), 263–340, Artech House, Boston, MA, 1998.